Experimental Determination of Lens Aberrations from the Intensity Point-Spread Function in the Focal Region

Peter Dirksen[a], Joseph Braat[b], Augustus J.E.M. Janssen[c],
Casper Juffermans[a] and Ad Leeuwestein[c]

[a]Philips Research Leuven, Belgium
[b]Delft University of Technology, The Netherlands
[c]Philips Research Laboratories, The Netherlands

ABSTRACT

In this paper we show various results of aberration retrieval using the pinhole method in conjunction with the extended Nijboer-Zernike theory. The experiments are performed on modern wafer scanners. Keyboard commanded offsets of the movable lens elements of the imaging tool have been used to introduce astigmatism, coma and spherical aberration in a controlled way. The method is designed to estimate these induced aberrations and we show the experimental results regarding the various types of aberrations created this way.

Keywords: Optical lithography, aberrations, phase retrieval, amplitude retrieval, point-spread function, extended Nijboer-Zernike theory

1. INTRODUCTION

In optical lithography, an exact knowledge of the point-spread function is required to calculate the image of an object. Projection lens aberrations cause the point-spread function to deviate from its ideal shape, that is well approximated by the Airy intensity distribution at moderate values of the numerical aperture (NA). The impact of lens aberrations on the image performance of the lens is well known and described by various authors.[1–4] To measure aberrations, several user tests exists, such as the in-situ interferometer[7] and those based on resist measurements.[8–10] The Extended Nijboer Zernike theory (ENZ)[5,6] provides an analytical expression for the point-spread function including the effects of defocus and aberrations. Due to the analytical nature of the formulas the ENZ theory is not only useful to do computations in the forward direction, i.e. to evaluate the point-spread function starting from aberrations, but also in the *reverse* direction, which amounts to aberration retrieval from the measured 3-D intensity point-spread function.

The pinhole method[11] is an experimental method to determine the aberrations of a wafer stepper or scanner in the factory, using the ENZ theory. The test pattern is an isolated transparent hole in a dark field binary mask. For a sufficiently small hole diameter, small compared to the system resolution, the image approximates the point-spread function of the lens, that is either recorded in resist or captured by a detector. The ENZ theory is flexible enough to allow for non-negligible pinhole sizes as well.

The pinhole method has a number of attractive features. The method is wavelength-independent and a single mask can be used on several systems. Due to the absence of phase errors in the mask, the determination of spherical aberration is likely to be more accurate compared to methods that use a phase shifting mask. Our method determines all aberrations: not only the phase errors of the projection lens but also the transmission errors can be determined in a single experiment. The pinhole method is a true projection lens test in the sense that its results are independent of the illuminator. One numerical aperture setting, the maximum NA, is needed

Further author information: (Send correspondence to P.D.)
P.D. and C.J.: E-mail: peter.dirksen@imec.be, Philips Research Leuven, Kapeldreef 75, B-3001 Leuven, Belgium
J.B.: Optics Research Group, Department of Applied Sciences, Delft University of Technology, Lorentzweg 1, NL-2628 CJ Delft, The Netherlands
A.J.E.M.J. and A.L.: Philips Research Laboratories, WY-81 and WY-51, NL-5656 AA Eindhoven, The Netherlands

to characterise the lens. Finally, no simulator is needed to calibrate the results since these directly translate into $m\lambda$ wave front aberration.

In this paper we show various results obtained on modern wafer scanners. Keyboard commanded offsets of the movable lens elements of the imaging tool have been used to introduce astigmatism, coma and spherical aberration in a controlled way. The pinhole method is designed to estimate these induced aberrations and we show the experimental results regarding the various types of aberrations created this way.

2. REVIEW OF THE EXTENDED NIJBOER ZERNIKE THEORY

In this section we briefly review the extended Nijboer-Zernike theory.[5,6] The general pupil function $A(\rho,\theta) \cdot exp\{i\Phi(\rho,\theta)\}$ of the projection lens with a possible non-constant transmission amplitude A is expanded as a series of Zernike terms Z_n^m:

$$A(\rho,\theta) \cdot exp\{i\Phi(\rho,\theta)\} = \sum_{n,m} \beta_{nm} Z_n^m(\rho,\theta) \tag{1}$$

The β_{nm} coefficients fully describe the lens. In Eq. 1 we generalize the more commonly used approach in which only the phase part Φ is expanded in a Zernike series. The uniqueness of the representation with the β_{nm} coefficients is guaranteed in practice by supposing sufficiently smooth functions A and Φ.

According to the ENZ theory, the through-focus complex amplitude of the point-spread function U is given by:

$$U(r,\phi,f) = 2\sum_{n,m} i^m \beta_{nm} V_{nm}(r,f) \cos m\phi \tag{2}$$

with analytically known V_{nm}; f is the axial 'defocus' coordinate and r the radial image plane coordinate, both in the appropriate diffraction units. The Zernike terms with a $\sin m\phi$-dependence have been omitted but are included in the full numerical treatment. The term V_{00} corresponds to the aberration-free case; it is assumed that β_{00} is positive and large compared to the other β_{nm}. The intensity $I(r,\phi,f)$ of the point-spread function after linearization can be written as a linear combination of basic intensity functions[11]:

$$\begin{aligned} I(r,\phi,f) &\approx 4\beta_{0,0}^2 |V_{00}(r,f)|^2 \\ &+ \beta_{0,0} \sum_{(n,m)\neq(0,0)} Im(\beta_{nm}) \Psi_n^m(r,f) \cos m\phi \\ &+ \beta_{0,0} \sum_{(n,m)\neq(0,0)} Re(\beta_{nm}) \chi_n^m(r,f) \cos m\phi \ . \end{aligned} \tag{3}$$

We have introduced here the basic intensity functions:

$$\Psi_n^m(r,f) = \gamma_m Re\{i^{m+1} V_{00}^* V_{nm}\} \ , \quad \chi_n^m(r,f) = \gamma_m Re\{i^m V_{00}^* V_{nm}\} \ . \tag{4}$$

with $\gamma_m = 4$, $m = 1,2,\cdots$, $\gamma_0 = 8$. Note the separation of r and ϕ terms in Eq. 3. Equation 3 consists of three parts: the first part is the aberration-free term, i.e. the through-focus Airy disk. The second part with the basic intensity functions Ψ_n^m and coefficients $Im(\beta_{nm})$ represents the phase errors of the lens. The third part with the basic intensity functions $\chi_n^m(r,f)$ and coefficients $Re(\beta_{nm})$ represents the transmission errors.

It can be shown that the finite hole size is correctly taken into account by replacing f by a complex defocus parameter throughout the formulas. Now a relatively large diameter may be used experimentally, significantly reducing the required exposure dose and making the experimental procedure much more practical. In the appendix the relation between the normalized and real space coordinates are presented, as well as a Bessel series representation of the V_{nm} functions that allow reliable computation of the V_{nm} for the relevant (r,f)-range and the correction of f to account for finite hole sizes is given.

Figure 1 shows the aberration-free point-spread function, or Airy pattern, $|V_{00}|^2$. The Airy pattern is an even function of the defocus parameter. Figure 2 shows a few examples of the basic functions Ψ_n^m and χ_n^m. The upper index m corresponds to the angular dependence. For example, the $m = 0$ term describes the rotationally

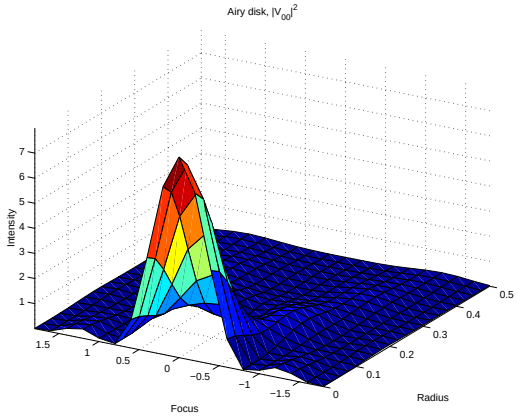

Figure 1: The Airy intensity pattern $|V_{00}(r, f)|^2$ as a function of the radial coordinate and defocus coordinate.

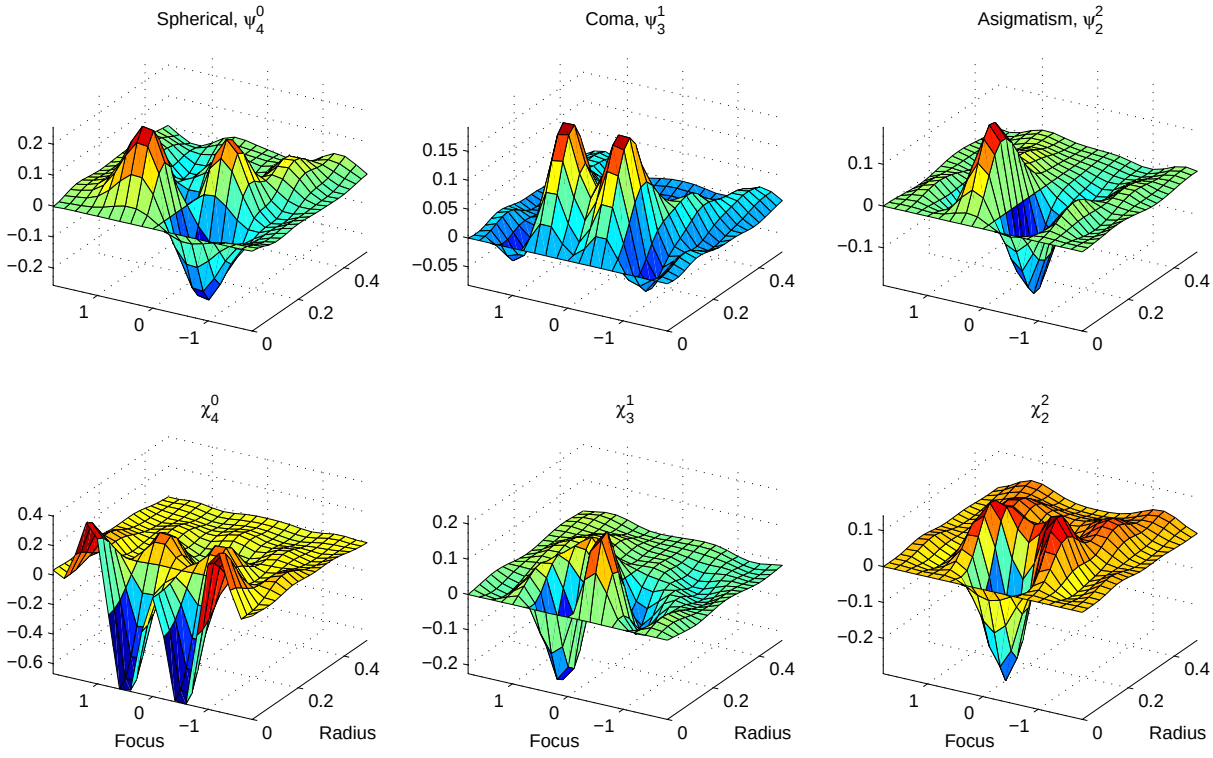

Figure 2. The dependence of the basic intensity functions on the radial coordinate r and defocus coordinate f. The top row shows the basic intensity functions corresponding to spherical, coma and astigmatism phase errors. The bottom row shows the corresponding basic functions associated with the transmission errors of the lens system. Note that $\Psi_n^m(r, f)$ and $\chi_n^m(r, f)$ have opposite through-focus symmetry.

symmetrical terms, i.e. spherical aberration. The coma terms correspond to $m = 1$, astigmatism to $m = 2$ and three-foil aberration to $m = 3$. Basic functions corresponding to higher order aberrations have larger values of n and tend to have a large radial and focus extent.

The basic functions Ψ_n^m and χ_n^m corresponding to phase errors and transmission errors, respectively, have opposite through-focus symmetry. As a consequence the phase errors and transmission errors can be separated

in an aberration retrieval experiment. The symmetry properties are summarised in the table below:

Through-focus symmetry properties (f-dependence)				
	m	n	Phase terms ψ_n^m	Transmission terms χ_n^m
Airy disk	0	0	even	
Spherical	0	$2, 4, \cdots$	odd	even
Tilt, Coma	1	$1, 3, 5, \cdots$	even	odd
Astigmatism	2	$2, 4, 6, \cdots$	odd	even
Three foil	3	$3, 5, 7, \cdots$	even	odd
$\vdots$				

In Fig. 3 we highlight the difference between a phase error and a transmission error. According to Eq. 3 the point-spread function of an aberrated lens is a linear combination of the aberration-free point-spread function V_{00} and Ψ_n^m and χ_n^m. As an example, Fig. 3 shows a point-spread function with astigmatism $m = 2$. The phase error produces the well-known elliptical deformation that changes its orientation when f is replaced by $-f$. In best focus, the basic function Ψ_2^2 vanishes and the point-spread function has quasi-rotational symmetry (higher order terms will produce a weak fourfold symmetry in best focus). Similarly, the transmission error produces an elliptical deformation. However, the ellipse maintains its orientation through focus and is present even in best focus.

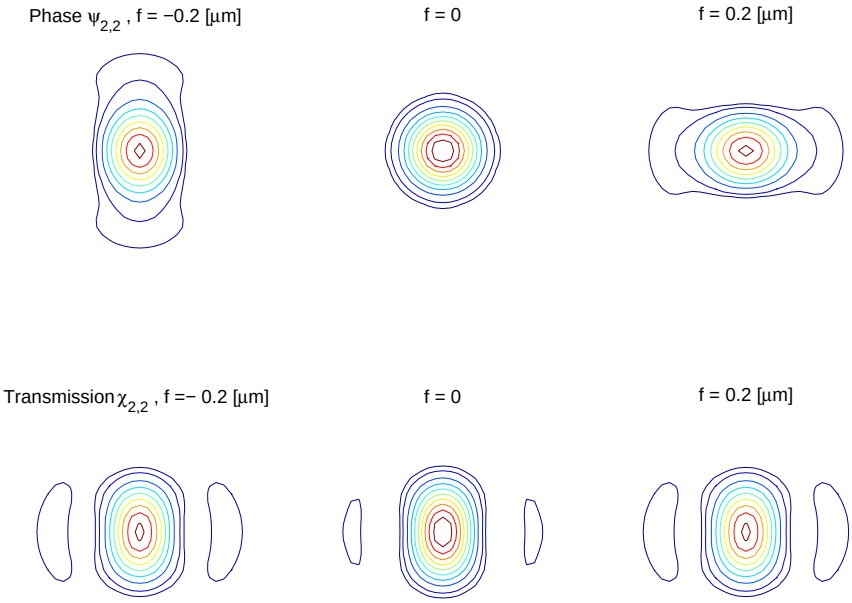

Figure 3. Point-spread function at three focus values in the presence of astigmatism $m = 2$. Top row: phase error, and bottom row: transmission error.

3. EXPERIMENTAL DETERMINATION OF THE POINT-SPREAD FUNCTION

We use a simple chrome-on-quartz reticle with $4 \times 0.15 = 0.6\,\mu m$ transparent holes. The same mask can be used for different scanners, even having a different exposure wavelength: an ASML PAS5500/750 system with $\lambda = 248$ nm, $NA = 0.70$ projection lens and an ASML PAS5500/950 system with $\lambda = 193$ nm, $NA = 0.63$ projection lens. The reticle is imaged onto a resist layer on a *SiON* anti-reflective coating. Using *SiON* instead of an organic anti-reflective coating has the advantage that it provides a good contrast in the SEM. First two

small reference marks are exposed, using the same reticle. The coordinate system, superimposed onto the image, is shown. In Fig. 4, the relatively large central image, represents a single contour of the intensity point-spread function at a certain exposure dose and defocus value. Inside this contour, the image intensity is above the resist threshold value and the resist completely develops away, leaving the $SiON$ layer. Outside the contour, the SEM image shows the undeveloped resist. The procedure is repeated for a number of focus values and exposure dose settings, i.e. the reticle is exposed in a focus exposure matrix (FEM). A SEM, under job control, collects all images. The data reduction is done off-line.

Figure 5 shows a superposition of a number of contours at a single defocus value. From these we have to estimate the coefficients β_{nm} of Eq. 1 of these basic functions that represent the pupil function. The coefficients are estimated by optimising the match between the theoretical intensity and the measured intensity $I(r, \phi, f)$ patterns at several values of the defocus parameter. However, at this point we only have resist contours as shown in Fig. 5 instead of complete intensity surfaces.

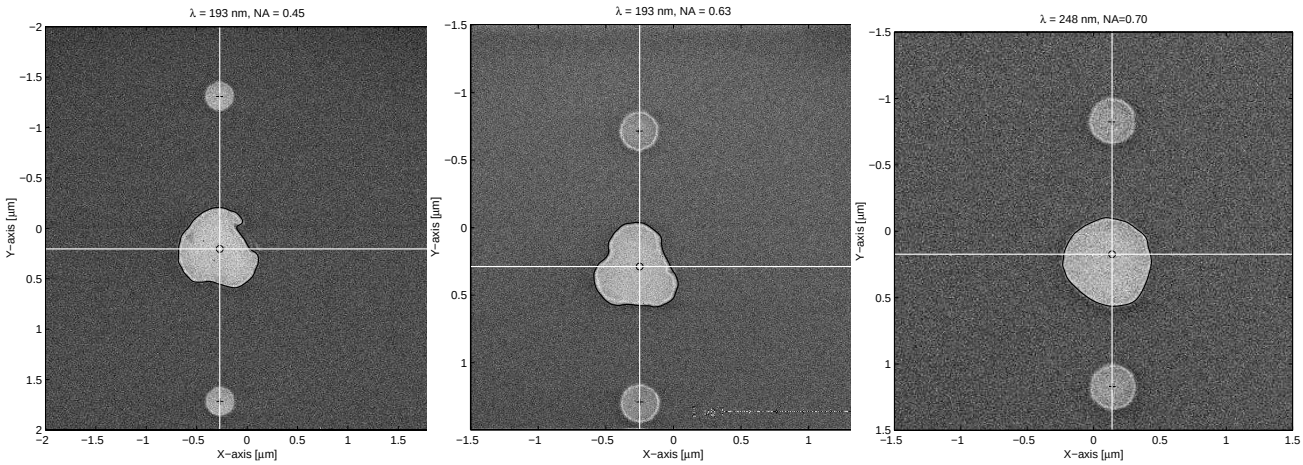

Figure 4. *This result illustrates the flexibility of the pinhole method. All experiments use the same mask and fixed hole size. Left: Scanner PAS5500-950, $\lambda = 193nm$ at NA = 0.45; central image NA=0.63. Right: PAS5500-700, $\lambda = 248nm$, NA =0.70.*

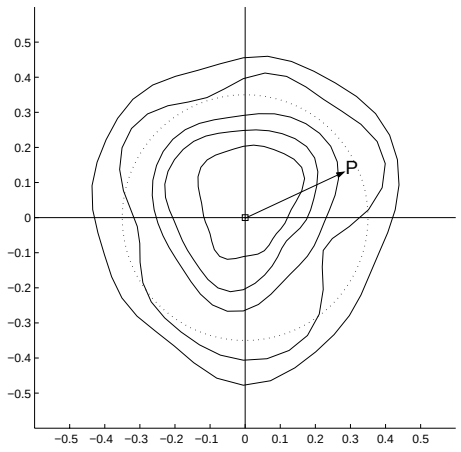

Figure 5. At one focus value a number of contours are combined into the intensity function. Scanner PAS5500-950, $\lambda = 193$nm, NA=0.63.

Effects of resist development and SEM effects are incorporated using a simple model. To convert the resist contours into the through-focus aerial image we have used a primitive model: a constant offset of 35 nm, which is an optimal value for our process, is removed from the diameter of all observed contours. An inaccuracy of this model will mainly impact the spherical transmission terms that are even through focus. But the phase terms with circular symmetry hardly suffer from the model inaccuracy, as is indeed proven by the experiments presented below. Along the corrected contours we now know the intensity of the point-spread function.

We will solve the unknown β's numerically by requiring optimal match between the right-hand side of Eq. 3 and the measured intensity profiles. The way we solve Eq. 3 involves a Fourier transform with respect to ϕ of both sides:

$$I^m(r,f) = \frac{1}{2\pi}\int_0^{2\pi} I(r,\phi,f)\cos m\phi d\phi \tag{5}$$

This requires availability of the intensity point-spread function $I(r,\phi,f)$ for general (r,ϕ) and not only on a finite number of contours. To approximate the value of I at a point for a given focus value, we discriminate between three cases. Inside the smallest contour we take I constant and equal to its value on that contour. Outside the largest contour, we take I constant and equal to its value on the largest contour. Between two contours we use linear interpolation to obtain values for I. We construct a path between the contours, that contains the point P. The beginning and end of the path are orthogonal to the contours. Along the constructed path we suppose I to be linear. For the numerical integration we only consider radial coordinate values smaller than the greatest value belonging to all contours.

Figure 6 shows examples of the experimentally determined radially symmetric part I^0. The radial symmetrical part is written as a linear combination of basic intensity functions with $m = 0$, i.e. $\Psi^{0,n}$ and $\chi^{0,n}$. Now two sets of linear equations have to be solved. The two sets of linear equations, corresponding to phase and transmission errors, decouple as $\Psi^{0,n}$ and $\chi^{0,n}$ have opposite parity with respect to their dependence on f. In this way the $\beta_{n,0}$ coefficients are easily estimated. Comparing the experimental intensity (solid lines) and

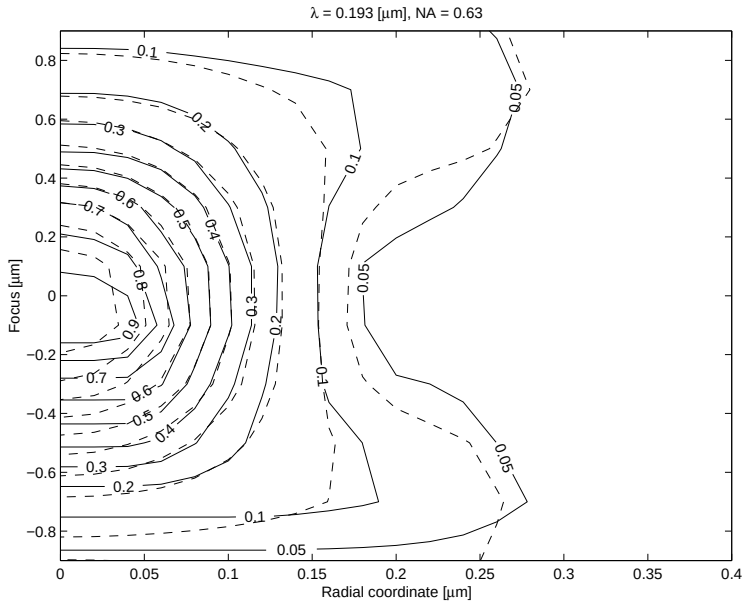

Figure 6. *The radially symmetrical part I^0 of the intensity point-spread function. Solid lines: experiment, dashed lines the retrieved intensity using the estimated $\beta_{n,0}$ coefficients. Scanner PAS5500-950, $\lambda = 193$nm, NA =0.63*

retrieved intensity using the estimate coefficients(dashed lines), the goodness of fit ($mean + 3\sigma$) is typically 8%. In a similar way the other aberrations like coma, astigmatism and three-foil are estimated from the observed Fourier components I^m for $m = 1, 2, 3$ respectively.

We have compared the results of the pinhole method with an independent aberration measurement according to the Aberration Ring Test.[9] The general picture is confirmed: the projection lens suffers from low order Y-coma, astigmatism and Y-oriented three-foil and only a small amount of other aberrations such as spherical is present. There is some similarity between ART and the new pinhole method: in the ART method a phase dot is exposed to resist, that prints as a ring. In the ideal case the ring has rotational symmetry and symmetry through focus. The shape deviations, in terms of Fourier components, are a measure for the different aberration types. After calibration with a simulator, the shape deviations can be translated into aberrations. The great advantage of the new method is that its result directly translates into transmission variation and wavefront aberration including a splitting into low and high order aberrations from a single experiment. Also note that the pinhole method uses one numerical aperture setting to characterise the lens.

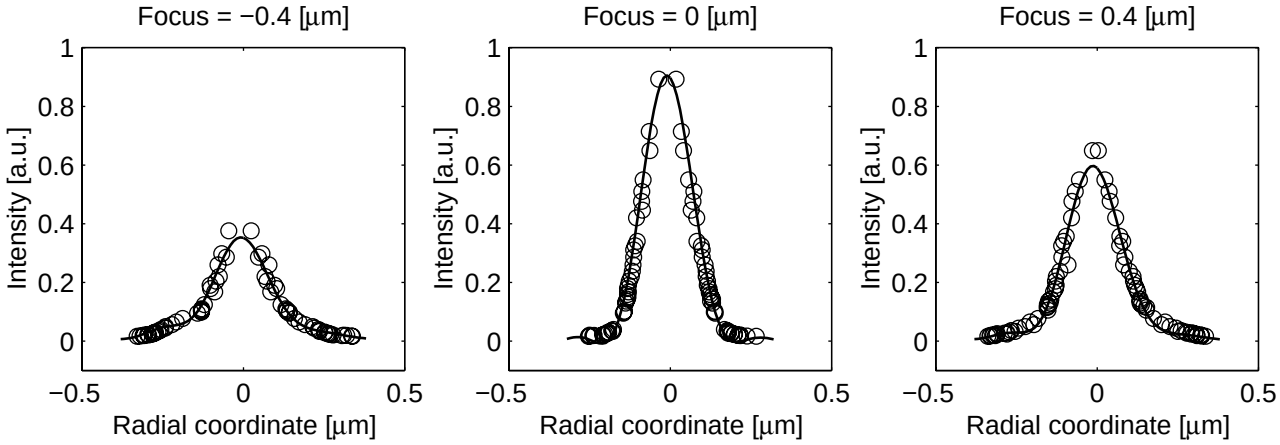

Figure 7. Through-focus cross-sections of the retrieved intensity PSF (solid) compared to the experimental PSF (circles).

4. DETUNING EXPERIMENT

The experimental result shown in Fig. 6 shows a good match between the experimental and retrieved intensity. A detuning experiment is used to validate the retrieved aberration parameters. We applied keyboard-commanded offsets of the movable lens elements, reticle table height and exposure wavelength of the imaging tool to introduce aberrations in a controlled way. The pinhole method is used to estimate these induced aberrations. The experimental results are summarised in Fig. 8 where we compare the nominal state of the imaging tool with a detuned state where the aberrations have been added. The measurements are performed at a single point near the edge of the imaging field.

The first experiment is shown in Fig. 8, top panel. Approximately 50 $m\lambda$ of spherical have been added and this detuned state is compared to the nominal state of the tool. The experiment confirms that only spherical aberration has changed while the other aberrations remain constant. The observed aberration change is approximately equal to the amount of spherical introduced to the system.

Similarly, Fig. 8 mid panel shows the result when 50 $m\lambda$ of X-coma have been added and Fig. 8 bottom panel shows the result when 50 $m\lambda$ of horizontal-vertical astigmatism have been added. At this moment we can estimate the wave front aberrations with a typical error of the order of 0.01λ.

5. SUMMARY AND DISCUSSION

In this paper we have shown various results of aberration retrieval using the pinhole method in conjunction with the extended Nijboer-Zernike theory. The detuning experiment, where commanded offsets of the movable lens elements have been used to introduce aberration, proves that the pinhole method is able to detect aberration

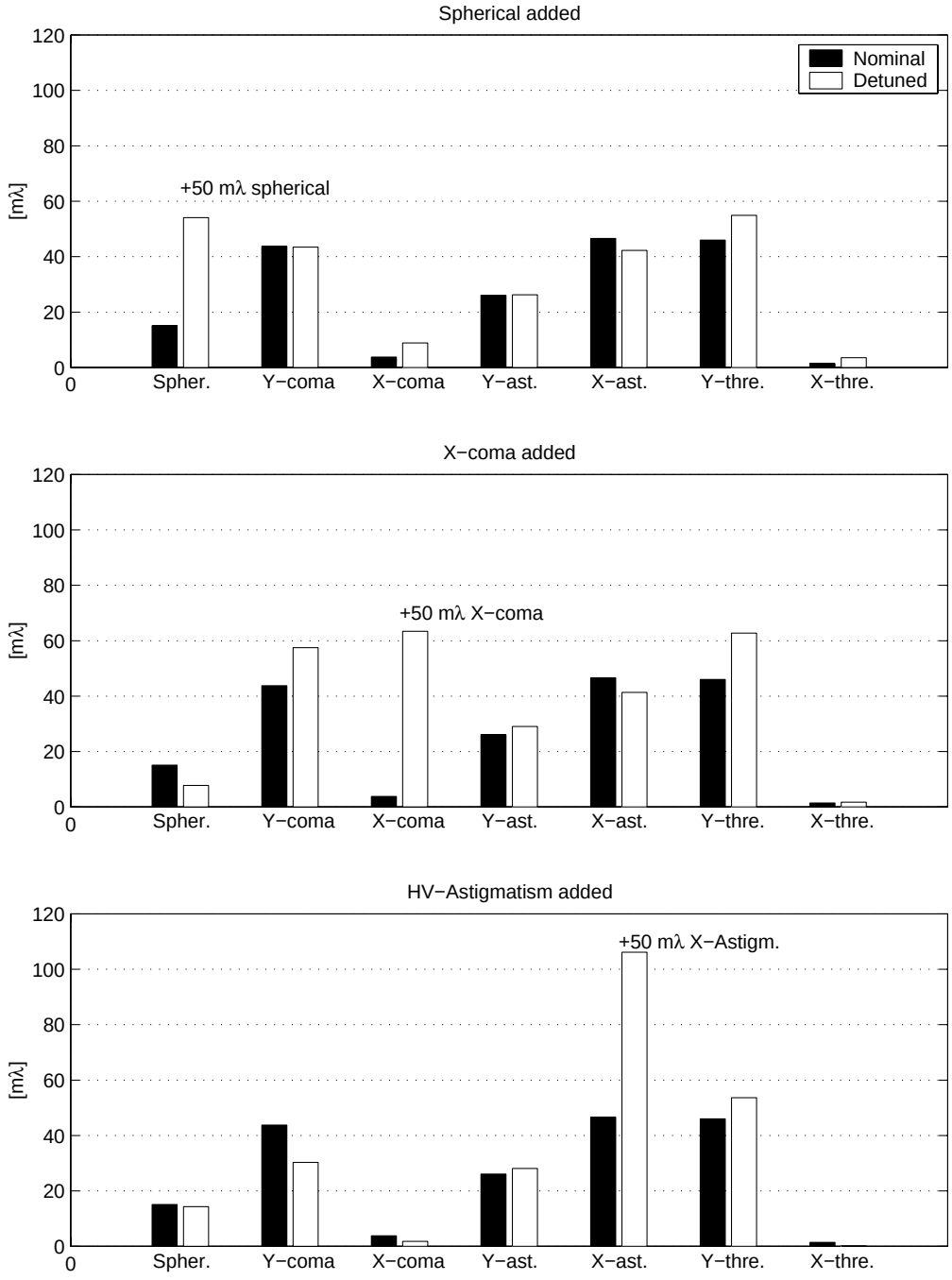

Figure 8. In the detuning experiment aberrations have been added to the imaging tool. The aberrations are retrieved and compared to the nominal state of the tool. Top: the nominal state is compared to a detuned state where +50 $m\lambda$ spherical aberration are added. Middle: nominal compared to the +50 $m\lambda$ X-coma state. Bottom: nominal compared to the +50 $m\lambda$ HV-astigmatism state.

changes. The pinhole method is wavelength-independent as was illustrated by the experimental results obtained on a DUV and a 193 nm scanner using the same reticle. In order to estimate the aberrations, no simulator was used to 'calibrate' the results, since these directly translate into $m\lambda$ wave front aberration simply by using the aberration retrieval procedure described above.

Some improvements are possible. To convert the resist contours into the through-focus aerial image we have used a primitive resist model: a constant offset is removed from the diameter of the observed contours. An inaccuracy of the resist model will mainly impact the spherical transmission terms that are even through focus. But the spherical phase terms, as is indeed proven by the experiments presented above, hardly suffer from the model inaccuracy. We also mention that we have used the linearized theory of Eq. 3 to estimate the aberrations. In principle it is possible to include the quadratic terms and to make a more accurate estimate of the lens errors.

ACKNOWLEDGMENTS

The authors wish to thank Hans Kwinten, David Van Steenwinckel, Michael Benndorf and Johannes van Wingerden from Philips Reseach Leuven and Peter de Bisschop from IMEC for their valuable input and experimental support.

6. APPENDIX

We briefly review the mathematics to calculate the point-spread function. A detailed description, including a description of aberration retrieval, is given elsewhere.[5, 6, 11] The relationship between normalised image coordinates (x, y) and the defocus parameter f on one hand and the real space image coordinates (X, Y, Z) in the lateral and axial direction on the other hand is given by:

$$\begin{aligned} x = X\frac{NA}{\lambda} \quad &, \quad y = Y\frac{NA}{\lambda} \\ r = \sqrt{x^2+y^2} \quad &, \quad (x,y) = (r\cos\phi, r\sin\phi) \\ f \quad &= \quad 2\frac{\pi}{\lambda}Z(1-\sqrt{1-NA^2}) \quad , \end{aligned} \tag{6}$$

with (r, ϕ) polar coordinates in the image plane. Finite hole size can be taken into account by replacing f by a complex defocus parameter $\approx f + i\pi^2/2a^2$ with a equal to the hole diameter.

For integers $n, m \geq 0$ with $n - m \geq 0$ and even, the Bessel series representation for the basic functions V_{nm} reads:

$$V_{nm}(r,f) = \exp(if)\sum_{l=1}^{\infty}(-2if)^{l-1}\sum_{j=0}^{p} v_{lj}\frac{J_{m+l+2j}(v)}{lv^l}, \; v = 2\pi r, \tag{7}$$

with v_{lj} given by

$$v_{lj} = (-1)^p(m+l+2j)\binom{m+j+l-1}{l-1}\binom{j+l-1}{l-1}\binom{l-1}{p-j}\Big/\binom{q+l+j}{l}, \tag{8}$$

where $l = 1, 2, \ldots;\; j = 0, \ldots, p$. In Eq. (8) we have set

$$p = \frac{n-m}{2} \quad , \quad q = \frac{n+m}{2}. \tag{9}$$

REFERENCES

1. T.A. Brunner, "Impact of lens aberrations on optical lithography", *Proceedings of the Microlithography Seminar Interface*, 1996 p. 1
2. D.G. Flagello, H. van der Laan, J. van Schoot, I. Bouchoms, B. Geh, "Understanding systematic and random CD variations using predictive modelling techniques", *Proceedings of the SPIE* **3679**, 1999 p. 162

3. C. Progler, D. Wheeler, "Optical lens specifications from the user's perspective", *Proceedings of the SPIE* **3334**, 1998, p.256
4. D. G. Flagello, B. Geh, "Lithographic lens testing: analysis of measured aerial images, interferometric data and photo resist measurements", *Proceedings of the SPIE* **2726** 1996, p.788
5. A.J.E.M. Janssen, "Extended Nijboer-Zernike approach for the computation of optical point-spread functions", *JOSA* **A 19**, 2002, p. 849
6. J.J.M. Braat, P. Dirksen, A.J.E.M. Janssen, "Assessment of an extended Nijboer-Zernike approach for the computation of optical point-spread functions", *JOSA* **A 19**, 2002, p. 858
7. N.R. Farrar, A.L. Smith, D. Busath, D. Taitano, "In-situ measurement of lens aberrations", *Proceedings of the SPIE* **4000**, 2000, p. 18
8. J.P. Kirk, T.A Brunner, "Measurement of microlithography aerial image quality", *Proceedings of the SPIE* **2726**, 1996, p. 410
9. P. Dirksen, C. Juffermans, A. Engelen, P. De Bisschop, H. Muellerke,"Impact of high order aberrations on the performance of the aberration monitor", *Proceedings of the SPIE* **4000**, 2000, p.9
10. F. Zach, C.Y. Lin, J.P Kirk, "Aberration analysis using reconstructed aerial images of isolated contacts on attenuated phase-shift masks", *Proceedings of the SPIE* **4346**, 2001 p. 1362
11. P. Dirksen, J. Braat, A.J.E.M. Janssen, C. Juffermans, "Aberration retrieval using the extended Nijboer-Zernike approach", J. Microlith. Microfab., Microsyst.,**2**, 2003, p. 61